# An electro-kinetic study of oxygen reduction in polymer electrolyte fuel cells at intermediate temperatures

Irene Gatto, Alessandro Stassi, Enza Passalacqua, Antonino Arico'

# An electro-kinetic study of oxygen reduction in polymer electrolyte fuel cells at intermediate temperatures

I. Gatto, A. Stassi, E. Passalacqua , A. S. Aricò*

*Institute for Advanced Energy Technologies, CNR-ITAE, via Santa Lucia Sopra Contesse, 5 -98126 – Messina (ME), Italy*

**Abstract**

The oxygen reduction process in polymer electrolyte fuel cells (PEMFCs) was in-situ investigated at intermediate temperatures (80 °-130 °C) by using a carbon supported PtCo catalyst and Nafion membrane as electrolyte. To overcome the Nafion dehydration above 100 °C, the experiments were carried out under pressurized conditions. Electro-kinetic parameters such as reaction order and activation energy were determined from the steady-state galvanostatic polarization curves obtained for the PEM single cell. Negative activation energies of 40 kJ $mol^{-1}$ and 18 kJ $mol^{-1}$ were observed at 0.9 V and 0.65 V, respectively, in the temperature range 100°-130 °C. This was a consequence of ionomer and membrane dry-out. The ionomer dry-out effect appears to depress reaction kinetics as the temperature increases above 100 °C since the availability of protons at the catalyst-electrolyte interface is linked to the presence of proper water contents. An oxygen reduction reaction of the first order with respect to the oxygen partial pressure was determined at low current densities. Maximum power densities of 990 $mWcm^{-2}$ and 780 $mWcm^{-2}$ at 100°C and 110°C ($H_2$-$O_2$) with 100% R.H., were achieved at 3 bars abs.

*Keywords:* Oxygen reduction reaction, Polymer electrolyte fuel cell, Pt-Co electrocatalyst, Intermediate temperature, Automotive.

* Corresponding author: Dr. A. S. Aricò, e-mail: arico@itae.cnr.it; phone: +39 090 624237, fax +39 090 624247.

## 1. Introduction

The oxygen reduction process is a limiting step in low temperature fuel cells and requires the use of noble metal catalysts such as Pt or Pt-alloys to occur at significant rates [1-20]. Large overpotentials (~0.5 V) are necessary to achieve a current density of about 1 A $cm^{-2}$ [10, 17]. This causes a loss of electrical efficiency of about 30-40 %. For such reason, the oxygen reduction reaction is one of the most studied processes for low temperature fuel cells [15]. Significant attention has been addressed to catalyst development, including reduction of the noble metal loading, and to study alternative catalysts as well as the reaction kinetics [10, 15]. Interestingly, the reaction rate does not increase significantly passing from polymer electrolyte fuel cell operation to phosphoric acid or phosphoric acid-doped polybenzimidazole fuel cells despite the increase of temperature from 80 °C to 180 °C [21-26]. The electrokinetic data reported in the literature reveal that the oxygen reduction reaction (ORR) is a thermal activated reaction; however, this is completely valid for specific temperature ranges [21, 22, 27]. Beside this aspect, several other factors such as electrolyte modifications occurring with temperature, blocking effect due to anion adsorption on catalytic sites, availability of water as necessary to transport active species to catalytic sites, e.g. protons, and oxygen solubility significantly affect this process [21, 22, 27-29].

PEMFCs are of relevant interest for automotive applications. One of the pre-requisites for such application is the possibility to operate the fuel cell in a wide temperature range from room temperature to around 120°- 130 °C [30]. Operation at 120 °C or 130 °C can mitigate the constraints concerning with thermal and water management allowing a simplification of the system and reducing the volume of the fuel cell system inside the car with a strong impact on costs and reliability [30]. Unfortunately, there are not so many polymer electrolytes that operate with constant performance in the range (80°-130 °C) and, at the same time, allow rapid and cold start-up. Some recent progress in this field includes the development of short side chain

perfluorosulfonic electrolyte membranes, composite membranes and novel polymer electrolytes [31-36].

To study the performance and stability of cathode electro-catalysts in the intermediate temperature range our group has recently carried out some studies related to the intermediate temperature operation at moderate pressures in the presence of short side chain perfluorosulfonic electrolyte membranes [30, 31, 37]. We have also investigated this process at temperatures comprised between 100° and 130 °C in the presence of conventional Nafion electrolytes by increasing the operation pressure thus avoiding membrane dehydration [17]. In these previous works, our attention was essentially focused on the performance and stability as well as on the impact of catalysts characteristics on these properties. The present study is focused on the effect of operating conditions such as temperature and pressure on the electro-kinetic parameters. Although the kinetics of the oxygen reduction process have been widely investigated in the low (up to 80 °C) or high temperature ranges (180 °C), limited efforts have been addressed to analyse the effect of operating conditions in the intermediate temperature range. An analysis of the effect of relevant physical factors may be appropriate to better understand the main drawbacks and provide useful information for tailoring novel electrolytes that can conveniently operate at intermediate temperatures. We have focused our efforts on the $Pt_3Co_1$ catalyst since a superior catalytic activity and stability with respect to conventional Pt/C catalysts has been demonstrated especially in the intermediate temperature range [37].

## 2. Experimental

### *2.1. Catalyst Preparation and characterization.*

The cathode catalysts consisted in a Ketjenbalck supported 50 wt % Pt-Co catalyst with nominal alloy composition $Pt_3Co_1$ (at.) whereas the anode catalyst was a 30 % Pt/Vulcan. These catalysts were prepared according to a previous work [37]. XRD analysis was carried out using a Philips X-pert 3710 X-ray diffractometer with Cu Ka radiation operating at 40 kV and 30 mA. The peak

profile of the (2 2 0) reflection in the face centered cubic structure of Pt was analysed by using the Marquardt algorithm and the crystallite size was calculated by the Debye–Scherrer equation. The degree of alloying was determined from the peak shift. TEM analysis was made by first dispersing the catalyst powder in isopropyl alcohol. A few drops of these solutions were deposited on carbon film-coated Cu grids and analysed with a FEI CM12 microscope.

*2.2. Electrodes and MEAs preparation*

The electrodes were prepared by a spray technique as described elsewhere [38, 39]. In particular, the catalytic layer was obtained by mixing the electro-catalysts previously prepared, (30% Pt/C for anode and 50 wt % Pt-Co/C for cathode), with a 33% (wt/wt) Nafion alcoholic solution (Aldrich, 5% wt/wt), 20% (wt/wt) of ammonium carbonate (Carlo Erba) as a pore-former. A Pt loading of 0.3 mg $cm^{-2}$ was used for both anode and the cathode side. The catalytic ink was sprayed on the ELAT HT Gas Diffusion Layers (GDLs). MEAs were obtained by hot pressing the electrodes onto commercial Nafion 115 membrane at 125°C for 5 min. The membranes were previously purified in a 5% vol. $H_2O_2$ solution (Carlo Erba) and in a 1 M $H_2SO_4$ solution (Carlo Erba).

*2.3. Electrochemical studies*

Electrochemical studies in PEM were performed in a $H_2/O_2$ 5$cm^{-2}$ single cell in a temperature range between 80°C and 130°C, by varying the pressure from 1 to 3 bar abs. and at a relative humidity (R.H.) of 100%. A $H_2/O_2$ feed was used in order to evaluate simultaneously the single cell performance and the mass activity for the ORR. The flow rates were fixed at 2 and 1.5 times the stoichiometry value for oxygen and hydrogen processes, respectively. The single cell performance was investigated by steady-state galvanostatic measurements. The cell was connected to a fuel cell test station including an HP6051A electronic load and an AUTOLAB Metrohm Potentiostat/Galvanostat equipped with FRA and a 20A current booster. For cyclic voltammetry (CV) studies, humidified hydrogen was fed to the anode that operated as both counter and reference electrode, whereas, humidified nitrogen was fed to the cathode (working electrode). The sweep rate

was 150 mV $s^{-1}$. The electrochemical active surface area was determined by integration of CV profile in the hydrogen adsorption region after correction for double layer capacitance. Data were not corrected for ohmic drop and hydrogen cross-over.

**3. Results and discussion**

The XRD pattern of the PtCo/C catalyst is shown in Fig. 1. The catalyst showed a cubic (fcc) structure for Pt and hexagonal structure for carbon support. The crystallite size calculated by using the Debye–Sherrer equation was about 3 nm. This size is generally assumed as a suitable compromise in terms of specific activity and surface area [3, 40-42]. The content of Co in the alloy, as determined from the shift of the diffraction peaks to higher Bragg angles was approaching the nominal one [41]. In particular, the 220 reflection, used as reference, was shifted positively by about 2° (2θ) with respect to a conventional carbon supported Pt catalyst of similar crystallite size. TEM analysis (Fig. 1, inset) showed proper metal particle dispersion and good homogeneity. The TEM micrographs also showed that essentially round Pt particles were present on the surface of the carbon support [41-42]. The mean particle size derived by TEM (~3 nm) was essentially similar to that obtained by XRD. The Pt-Co catalyst surface area was measured by cyclic voltammetry in the single cell by feeding $N_2$ instead of $O_2$ at the cathode. The CV profile is shown in Fig. 2. An electrochemical active surface area (ECSA) of about 47 $m^2\ g^{-1}$ was determined from the charge associated to the hydrogen adsorption and desorption peaks. If we consider that the theoretical geometrical metal surface area for round particles with 3 nm particle size is around 93 $m^2\ g^{-1}$ [31], the catalyst utilization in the polymer electrolyte single cell configuration is about 50%.

The effect of pressure on single cell performance at 80°C and 100% RH is shown in Fig. 3a-b. As expected, the performance progressively decreases by reducing the pressure from 3 bar to 1 bar abs. It is evident that the effect of pressure increases mainly as the current density increases; however, it affects essentially all regions of the polarization curves (activation, ohmic and mass transport controlled regions) [43]. The effect of the pressure was relevant in the mass transport controlled region affecting the limiting current density and maximum power density. The maximum

power densities were 643 $mWcm^{-2}$ and 853 $mWcm^{-2}$ at 1 and 3 bar abs., respectively. Less relevant but in any case significant was the effect of pressure in the intermediate current region which, in general, is of more interest for practical operation at a suitable electric efficiency. A voltage loss of about 100 mV at 1 A $cm^{-2}$ was recorded passing from 3 bar to 1 bar abs, with a consequent decrease of maximum power density of about 100 $mWcm^{-2}$

Fig. 4a-b shows the influence of temperature on performance under high pressure (3 bar abs) operating conditions. At this pressure, the performance level at 80°C and 100°C was similar with a maximum power density of 934 $mWcm^{-2}$ and 990 $mWcm^{-2}$, respectively. It is important to point out that at high pressure there is a good fraction of liquid water inside the membrane and the catalytic layers even at temperatures above 100 °C. Thus the operating conditions for the electrolyte in terms of water content are not significantly different.

A slight decrease in performance was detected at 110°C. In fact, at this operative condition, a cell potential of 510 mV at 1.5 A $cm^{-2}$ was reached, with a decrease of about 80 mV compared to that obtained at lower temperatures. A different trend was observed at 130 °C, where a drastic reduction in performance was detected. A maximum power density of only 490 $mWcm^{-2}$, about 500 $mWcm^{-2}$ lower than that obtained under the best operating conditions (100°C), was reached. Thus, despite the increase of pressure, a consistent performance drop was recorded at 130 °C with a conventional perfluorosulfonic acid membrane indicating that the system suffered of significant dehydration effects both involving membrane and ionomer. The water generated by the fuel cell reaction produced some internal humidification at 130 °C; but, this did not appear sufficient to recover the performance. On the other hand the performance at 110 °C appeared acceptable provided that an appropriate pressure was used.

Single cell electrochemical data obtained under different operative conditions were used to derive the electro-kinetic parameters such as mass activity ($j_m$, mA $mg^{-1}$) and specific activity ($j_s$, μA $cm^{-2}$) at two different cell potential (0.9 V and 0.65 V). Of course, at 0.9 V, these values reflect a kinetic controlled regime whereas at 0.65 V there is an affect of ohmic and mass transfer losses.

Fig.5a-d shows the variation of $j_m$ and $j_s$ at 0.9 V and 0.65 V as a function of the operating pressure and at 80 °C. It is evident an almost linear trend for mass and specific activity at both operating potentials. At 0.9 V, from the mass activity trend, the reaction order for the ORR is approaching 1 in the investigated range of oxygen pressure. Whereas at 0.65 V, the effects of ohmic and mass transport control cause the occurrence of a lower reaction order of about 0.7. This would indicate that the influence of oxygen pressure on the reaction rate, under constant potential, is indeed more relevant in the activation controlled region than in the region where ohmic and mass transport effects are dominant. Whereas, we have previously evidenced that, at a constant reaction rate (constant current), the potential loss in the polarization curves was more relevant in the ohmic and mass transport controlled regions. In order to understand the practical implications of these two evidences, it is useful to remember that a fuel cell system is generally operated at suitably high current to reduce capital costs. However, a high operating pressure will involve an excessive energy consumption on the gas compressor. Thus, a compromise is always necessary.

The influence of the operating temperature on mass and specific activity at a constant pressure (3 bar abs) is shown in Fig. 6a-d. It is noticeable a slope change passing from 80°C-100°C to the region 100°C-130°C. This behaviour indicates a different reaction mechanism depending on the range of temperature in which the catalyst operates. This effect appears clearly determined by the fact that both Nafion membrane and ionomer in the catalytic layer undergo to dehydration phenomena. At 0.9 V, there is no change in mass and specific activity up to 100 °C whereas both parameters decrease linearly in the range 100 ° C- 130 °C with a slope of -5 mA/mg catalyst per degree centigrade. The slope is also relevant at 0.65 V since the ohmic drop associated to the membrane dehydration adds to the effect ionomer dry out in a region where the activation control is generally less relevant. These results indicate that it is necessary to develop both membrane and ionomers for intermediate temperature operation. However, these novel electrolytes should also maintain appropriate ion conduction characteristics at conventional temperatures.

The Arrhenius plot for the ORR at the PtCo/C catalyst is reported in Fig.7 at both 0.9 V and 0.65 V. Negative activation energies ($E_a$) of -40 kJ $mol^{-1}$ and -18 kJ $mol^{-1}$ were calculated at 0.9 V and 0.65 V, respectively. These values represent the increase of activation energy as a function of temperature and at a constant pressure for the ORR as a consequence of membrane and ionomer dry-out in the presence of a Nafion electrolyte. This may be assumed as a baseline to establish the progress beyond the state of the art for the novel ionomers for automotive applications [44]. In fact, beside the increase of conductivity and performance in the intermediate temperature range, the beneficial effects introduced by any novel electrolyte may be also assessed in terms activation energy and mass activity for a specific catalyst.

**4. Conclusions**

The oxygen reduction kinetics were investigated in a polymer electrolyte fuel cell in the intermediate temperature range i.e. 80 °- 130 °C to get information about the catalyst operation under automotive conditions. For this study, a $Pt_3Co_1$ catalyst characterised by suitable suface area and degree of alloying was used. Mass activity and specific activity decreased in the range 100°-130 °C whereas a positive reaction order (first order) with respect to the pressure at low current density was recorded. Negative activation energies were observed both in the activation and ohmic drop controlled regions revealing that both ionomer and membrane dry-out phenomena played a relevant role at intermediate temperatures. In general, the ionomer dry-out effect reduces the availability of the protons at the catalyst-electrolyte interface whereas the membrane dehydration affects proton transport and thus increases the ohmic drop. By increasing the pressure up to 3 bars abs, appropriate performances were registered up to 110 °C with Nafion. Novel electrolyte membranes for intermediate temperature operation should address both the extension of the operating temperature range up to 130 °C and the decrease of pressure down to 1.5 bar abs as required for automotive applications.

**Acknowledgements**

The authors acknowledge the financial support of the EU through the QuasiDry Project 256821. "The research leading to these results has received funding from the European Community's Seventh Framework Programme (FP7/2010-2013) under the call ENERGY-2010-10.2-1: Future Emerging Technologies for Energy Applications (FET)."

**References**

[1] Jalan V, Taylor EJ. Importance of interatomic spacing in catalytic reduction of oxygen in phosphoric acid. J. Electrochem. Soc. 1983;130:2299-302.

[2] Beard BC, Ross PN, The structure and activity of Pt-Co alloys as oxygen reduction electrocatalysts. J. Electrochem. Soc. 1990;137:3368-74.

[3] Giordano N, Passalacqua E, Pino L, Arico AS, Antonucci V, Vivaldi M, Kinoshita K. Analysis of platinum particle-size and oxygen reduction in phosphoric-acid. Electrochim. Acta 1991;36:1979–84.

[4] Stassi A., Gatto I., Monforte G., Baglio V., Passalacqua E., Antonucci V., Aricò AS.

The effect of thermal treatment on structure and surface composition of PtCo electro-catalysts for application in PEMFCs operating under automotive conditions. J. Power Sources 2012; 208:35-45.

[5] Freund A, Lang J, Lehman T, Starz KA. Improved Pt alloy catalysts tor fuel cells Cat. Today 1996;27:279-83.

[6] Toda T, Igarashi H, Watanabe M, Enhancement of the electrocatalytic $O_2$ reduction on Pt-Fe alloys J. Electroanal. Chem. 1999;460:258-62.

[7] Mukerjee S, Srinivasan S, Soriaga MP, McBreen J. Effect of preparation conditions of Pt alloys on their electronic structural and electrocatalytic activites for oxygen reduction. XRD, XAS and eelctrochemical studies. J. Electrochem. Soc. 1995;142:1409-22.

[8] Min M-K, Cho J, Cho K, Kim H. Particle size and alloying effects of Pt-based alloy catalysts for fuel cell applications. Electrochimica Acta 2000; 45:4211–17.

[9] Antoine O, Bultel Y, Durand R. Oxygen reduction reaction kinetics and mechanism on platinum nanoparticles inside Nafion. J. Electroanal. Chem. 2001; 499:85–94.

[10] Gasteiger HA, Kocha SS, Sompalli B, Wagner FT. Activity Benchmarks and Requirements for Pt, Pt-Alloys, and Non-Pt Oxygen Reduction Catalysts for PEMFCs. Appl. Catal. B: Environ. 2005;56:9–35.

[11] Salgado JRC, Antolini E, Gonzalez ER, Structure and activity of carbon-supported Pt - Co electrocatalysts for oxygen reduction J. Phys. Chem. B 2004;108:17767-74.

[12] Jaffray C, Hards GA. in: Vielstich W, Lamm A, Gasteiger H. (Eds.), Handbook of Fuel Cells Fundamentals, Technology and Applications, vol. 3, Wiley, Chichester, UK, 2003, p. 509 (Chapter 41).

[13] Scholta J, Berg N, Wilde P, Jorissen L, Garche J, Development and performance of a 10 kW PEMFC stack. J. Power Sources 2004;127:206–12.

[14] Stamenkovic VR, Mun BS, Arenz M, Mayrhofer KJJ, Lucas CA, Wang G, Ross PN, Markovic NM. Trends in electrocatalysis on extended and nanoscale Pt-bimetallic alloy surfaces. Nat. Mater. 2007;6:241-47.

[15] Zhang S, Yuan X.-Z, Hin JNC, Wang H, Friedrich K A, Schulze M, A review of platinum-based catalyst layer degradation in proton exchange membrane fuel cells J. Power Sources 2009; 194:588–600.

[16] Strasser P, Koh S, Anniyev T, Greeley J, More K, Yu C, Liu Z, Kaya S, Nordlund D, Ogasawara H, Toney MF, Nilsson A, Lattice-strain control of the activity in dealloyed core-shell fuel cell catalysts. Nat. Chem. 2010;2:454-60.

[17] Aricò AS, Stassi A, Modica E, Ornelas R, Gatto I, Passalacqua E, Antonucci V. Performance and degradation of high temperature polymer electrolyte fuel cell catalysts J. Power Sources 2008;178:525-36.

[18] Borup RL, Davey JR, Garzon FH, Wood DL, Inbody MA, PEM fuel cell electrocatalyst durability measurements J. Power Sources 2006;163:76–81.

[19] Colon-Mercado HR, Popov BN. Stability of platinum based alloy cathode catalysts in PEM fuel cells. J. Power Sources 2006; 155:253–63.

[20] Duong HT, Rigsby MA, Zhou W-P, Wieckowski A, Oxygen reduction catalysis of the Pt3Co alloy in alkaline and acidic media studied by X-ray photoelectron spectroscopy and electrochemical methods. J. Phys. Chem. C 2007;111:13460-65.

[21] Zelenay P, Scharifker BR, Bockris JO'M. Comparison of he properties of $CF_3SO_3H$ and $H_3PO_4$ in relation to fuel cells. J. Electrochem. Soc. 1986;133:2262-67.

[22] Parthasarathy A, Srinivasan S, Appleby A J, Martin C R. Temperature Dependence of the Electrode Kinetics of Oxygen Reduction at the Platinum/Nafion® Interface-A Microelectrode Investigation. J. Electrochem. Soc., 1992; 139: 2530-37

[23] Kunz HR, Gruver GA. Catalytic activity of Platinum supported on carbon for electrochemical reduction of oxygen in phosphoric acid. J. Electrochem. Soc. 1975;122:1279-87.

[24] Maggio G. Modelling of phosphoric acid fuel cell cathode behaviour. J. Appl. Electrochem. 1999;29:171-76.

[25] Yang SC, Cutlip MB, Stonehart P. Simulation and optimization of porous gas-diffusion electrodes used in hydrogen/oxygen phosphoric acid fuel cells-I. Application of cathode model simulation and optimization to PAFC cathode development. Electrochim. Acta 1990; 35:869-78.

[26] Li Q, Jensen JO, Pan C, Bandur V, Nilsson MS, Schönberger F, Chromik A, Hein M, Häring T, Kerres J, Bjerrum NJ. Partially fluorinated arylene polyethers and their ternary blends with PBI and H3PO4. Part II. Characterisation and fuel cell tests of the ternary membranes. Fuel Cells 2008;8:188-99.

[27] Giordano N, Aricò AS, Hocevar S, Staiti P, Antonucci PL, Antonucci V. Oxygen reduction kinetics in phosphotungstic acid at low temperature Electrochim. Acta, 1993;38:1733-41.

[28] Aricò AS, Antonucci V, Alderucci V, Modica E, Giordano N. A.c.-impedance spectroscopy study of oxygen reduction at Nafion® coated gas-diffusion electrodes in sulphuric acid. J. Applied Electrochem. 1993; 23:1107-16.

[29] Aricò AS, Alderucci V, Antonucci V, Ferrara S, Recupero V, Giordano N, Kinoshita K, Ac-Impedance spectroscopy of porous gas diffusion electrode in sulphuric acid. Electrochimica Acta 1992;37:523-29.

[30] Aricò AS, Di Blasi A, Brunaccini G, Sergi F, Dispenza G, Andaloro L, Ferraro M, Antonucci V, Asher P, Buche S, Fongalland D, Hards GA, Sharman JDB, Bayer A, Heinz G, Zandonà N, Zuber R, Gebert M, Corasaniti M, Ghielmi A, Jones DJ. High Temperature Operation of a Solid Polymer Electrolyte Fuel Cell Stack Based on a New Ionomer Membrane. Fuel Cells 2010;10:1013–23.

[31] Stassi A, Gatto I, Passalacqua E, Antonucci V, Aricò AS, Merlo L, Oldani C, Pagano E, Performance comparison of long and short-side chain perfluorosulfonic membranes for high temperature polymer electrolyte membrane fuel cell operation. J. Power Sources 2011; 196:8925-30.

[32] Kreuer KD. On the development of proton conducting materials for technological applications. Solid State Ionics 1997;97:1–15.

[33] Aricò AS, Baglio V, Di Blasi A, Modica E, Antonucci PL, Antonucci V. Surface properties of inorganic fillers for application in composite membranes-direct methanol fuel cells. Journal of Power Sources 2004;128:113-8.

[34] Alberti G, Casciola M, Annu. Rev. Mater. Res. 2003; 33:129–54.

[35] Li Q, He R, Jensen JO, Bjerrum NJ, Chem. Mater. 2003;15:4896–915.

[36] Peron J, Nedellec Y, Jones DJ, Rozière J. J. Power Sources 2008;185:1209-17.

[37] Aricò AS, Stassi A, Gatto I, Monforte G, Passalacqua E, Antonucci V. Surface properties of Pt and PtCo electrocatalysts and their influence on the performance and degradation of high-temperature polymer electrolyte fuel cells. J. Phys. Chem. C 2010; 114:15823–36.

[38] Gatto I, Saccà A, Carbone A, Pedicini R, Urbani F, Passalacqua E. CO-tolerant electrodes developed with PhosphoMolybdic Acid for Polymer Electrolyte Fuel Cell (PEFCs) application. J. Power Sources 2007; 171:540-5.

[39] Gatto I, Saccà A, Carbone A, Pedicini R, Passalacqua E, MEAs for polymer electrolyte fuel cell (PEFC) working at medium temperature J. Fuel Cell Science and Technology. 2006;3:361-5.

[40] Yang D , Li B, Zhang H Ma. J. Kinetics and electrocatalytic activity of IrCo/C catalysts for oxygen reduction reaction in PEMFC. Int J Hydrogen Energy 2012; 37:2447-54.

[41] Kim JW, Heo JH, Hwang SJ, Yoo SJ, Jang JH, Ha JS, Jang S, Lim T.-H, Nam SW, Kim S-K.

Effects of stabilizers on the synthesis of Pt3Cox/C electrocatalysts for oxygen reduction. Int J Hydrogen Energy. 2011; 36:12088-95.

[42] Popov BN, Li X, Liu G, Lee J-W. Power source research at USC: Development of advanced electrocatalysts for polymer electrolyte membrane fuel cells. Int J Hydrogen Energy. 2011;36:1794-1802.

[43] Gonnet AE, Robles S, Moro L. Performance study of a PEM fuel cell

Int J Hydrogen Energy. 2012 Article in Press: http://dx.doi.org/10.1016/j.ijhydene.2011.12.076.

[44] Kang S, Min K, Mueller F, Brouwer J. Configuration effects of air, fuel, and coolant inlets on

the performance of a proton exchange membrane fuel cell for automotive applications. Int J Hydrogen Energy. 2009; 34:6749-64.

**Captions to Figures**

**Fig. 1 – XRD patterns of carbon 50 wt% Pt-Co electrocatalyst; the inset shows a TEM micrograph of the sample.**

**Fig. 2 – In situ cyclic-voltammetry of the PtCo/C with $H_2$ feed at counter and reference electrode and $N_2$ feed at the working electrode. Sweep rate 150 mV $s^{-1}$.**

**Fig. 3 – (a) Polarisation curves at 80 °C and different pressure for the Pt-Co/C catalyst. (b) Power density curves at 80 °C and different pressure for the Pt-Co/C catalyst.**

**Fig. 4 – (a) Polarisation curves at different cell temperatures and 3 bar abs for the Pt-Co/C catalyst. (b) Power density curves at different cell temperatures and 3 bar abs for the Pt-Co/C catalyst**

**Figure 5 – Variation of mass activity ($j_m$) as a function of pressure at 80°C at 0.9 V (a) and 0.65 V (b) . Variation of specific activity ($j_s$) as a function of pressure at 80°C at 0.9 V (c) and 0.65 V (d).**

**Fig. 6 – Variation of mass activity ($j_m$) as a function of temperature at 3 bar abs at 0.9 V (a) and 0.65 V (b) . Variation of specific activity ($j_s$) as a function of pressure at 80°C at 0.9 V (c) and 0.65 V (d).**

**Fig. 7 – Arrhenius plot for the ORR mass activity ($j_m$) at 0.9 V and 0.65 V at a Pt-Co/C electrocatalyst (3 bar abs.).**

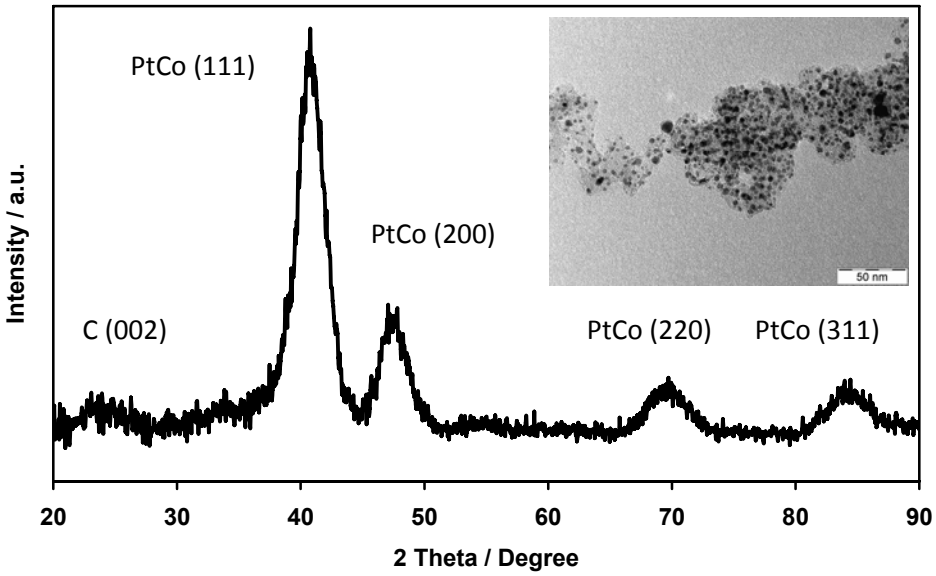
PtCo (111)
PtCo (200)
C (002)
PtCo (220)
PtCo (311)
50 nm
Intensity / a.u.
20
30
40
50
60
70
80
90
2 Theta / Degree

Figure 1

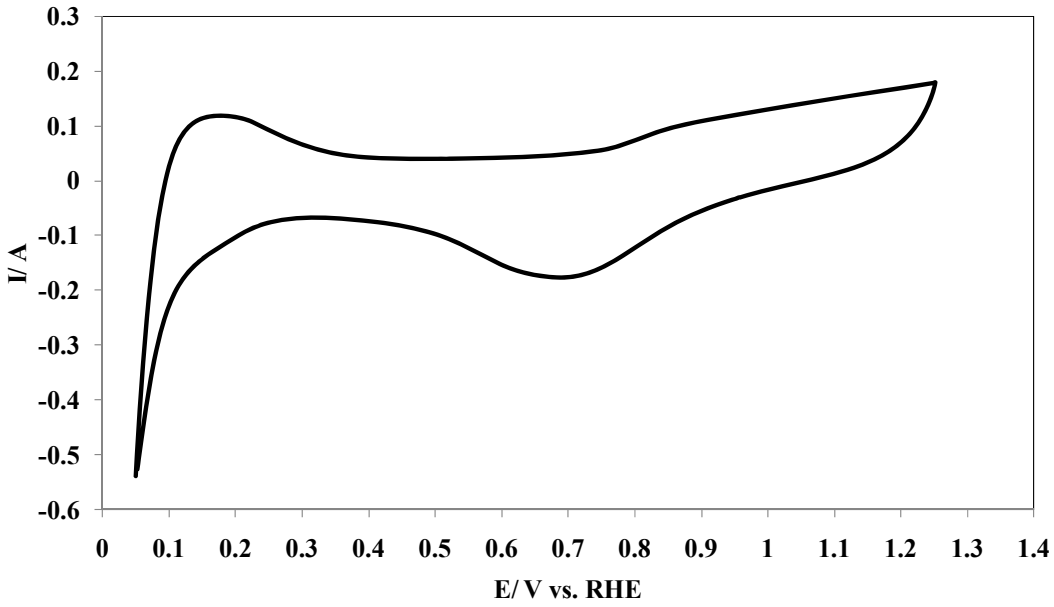
0.3
0.2
0.1
0
-0.1
-0.2
-0.3
-0.4
-0.5
-0.6
I/ A
0
0.1
0.2
0.3
0.4
0.5
0.6
0.7
0.8
0.9
1
1.1
1.2
1.3
1.4
E/ V vs. RHE

Figure 2

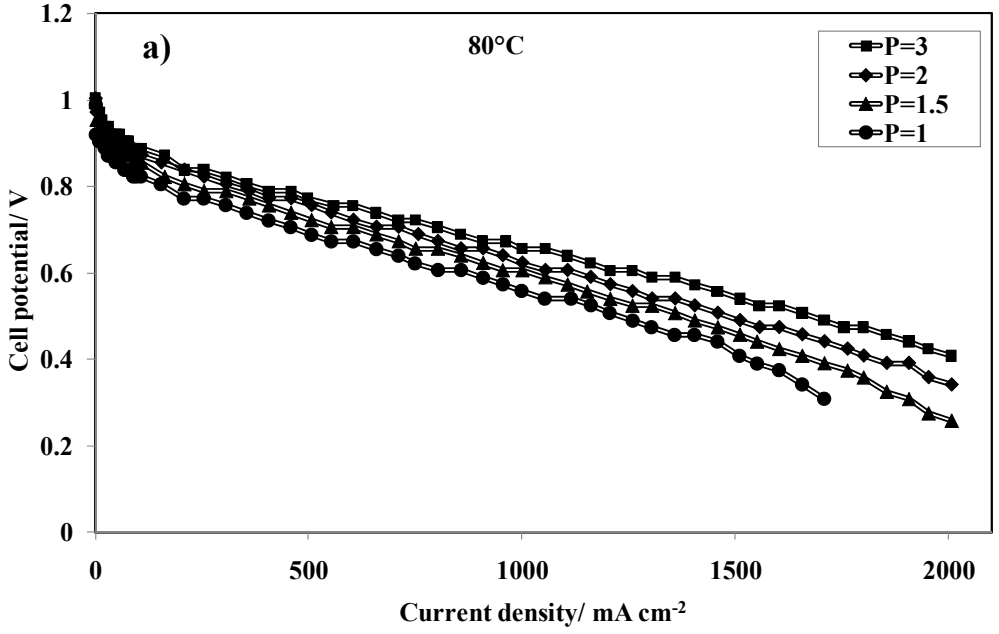
a)
80°C
P=3
P=2
P=1.5
P=1
Cell potential/ V
Current density/ mA cm-2
0
0.2
0.4
0.6
0.8
1
1.2
0
500
1000
1500
2000

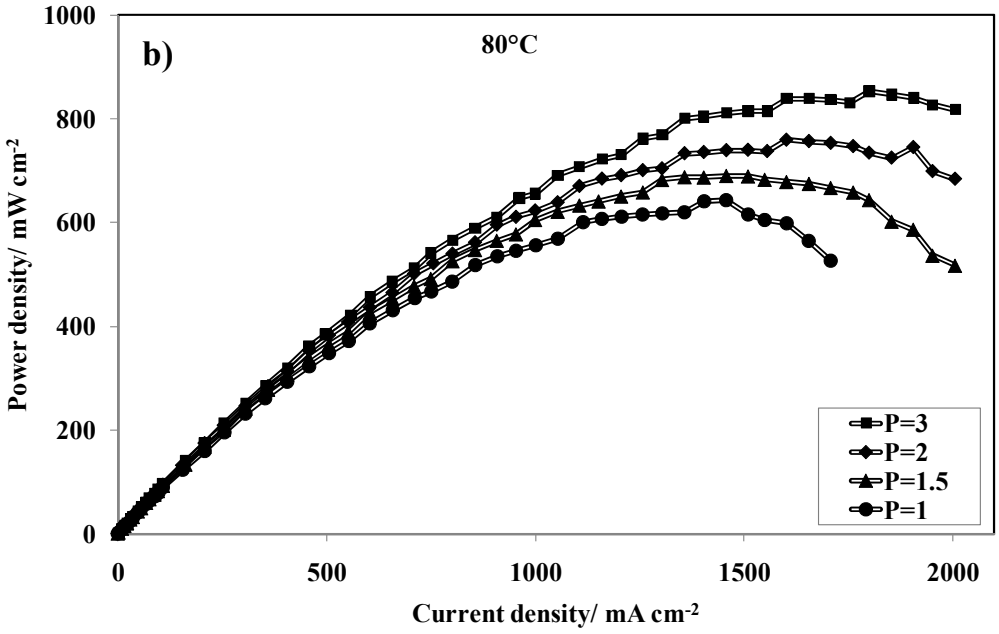
b)
80°C
P=3
P=2
P=1.5
P=1
Power density/ mW cm-2
Current density/ mA cm-2
0
200
400
600
800
1000
0
500
1000
1500
2000

Figure 3

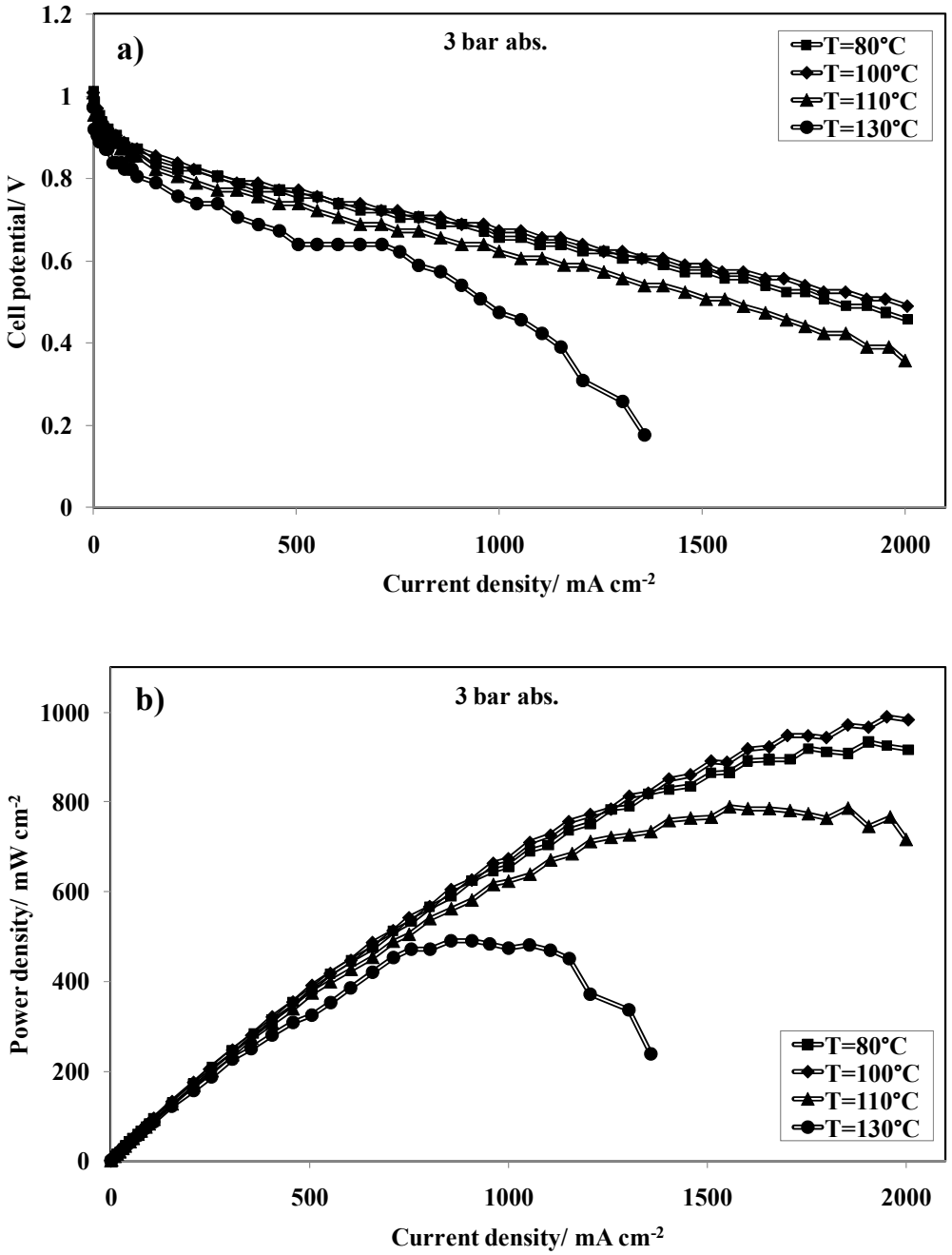
a)
3 bar abs.
T=80°C
T=100°C
T=110°C
T=130°C
Cell potential/ V
Current density/ mA cm-2
b)
3 bar abs.
Power density/ mW cm-2
Current density/ mA cm-2

Figure 4

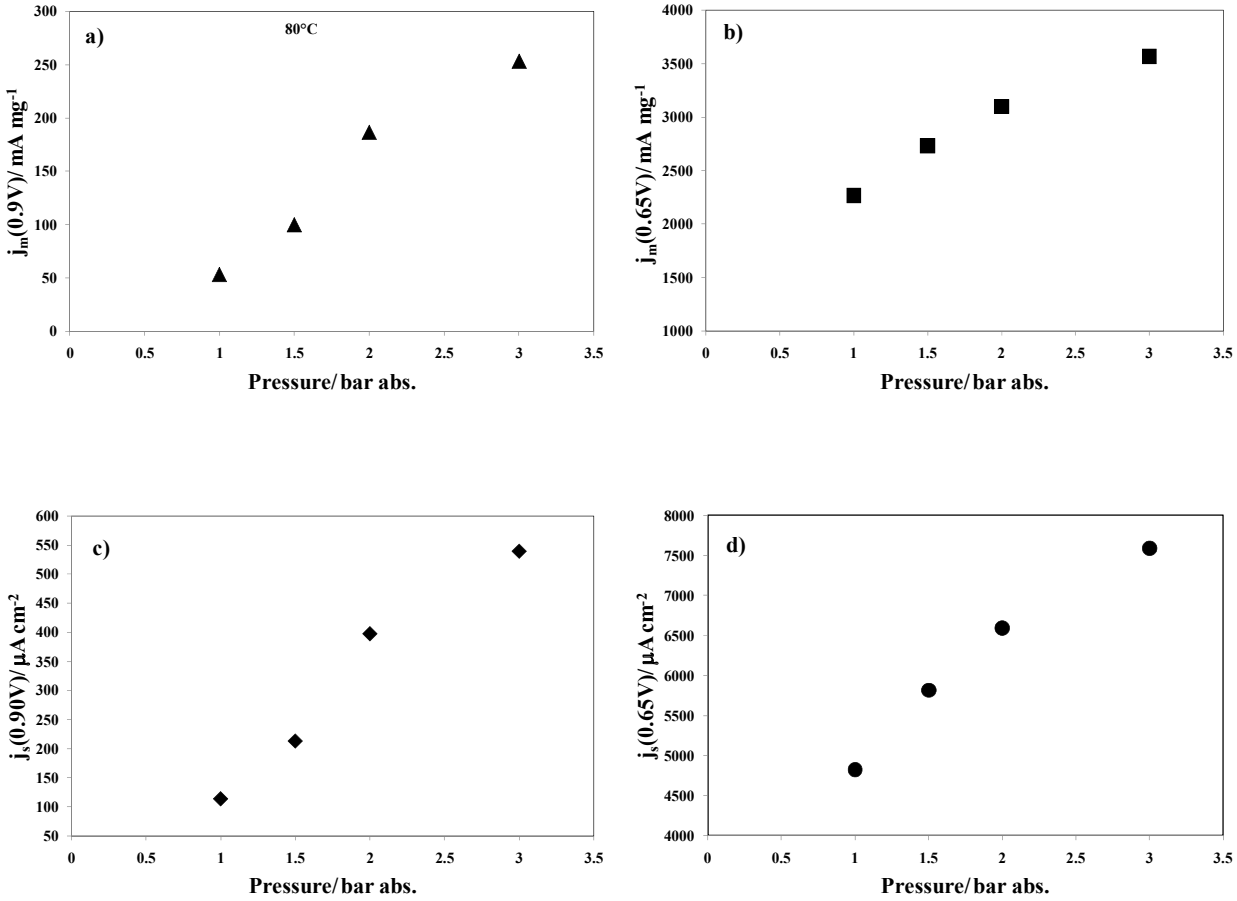
a)
80°C
$j_m$(0.9V)/ mA mg$^{-1}$
Pressure/ bar abs.
b)
$j_m$(0.65V)/ mA mg$^{-1}$
Pressure/ bar abs.
c)
$j_s$(0.90V)/ µA cm$^{-2}$
Pressure/ bar abs.
d)
$j_s$(0.65V)/ µA cm$^{-2}$
Pressure/ bar abs.

Figure 5 a-d

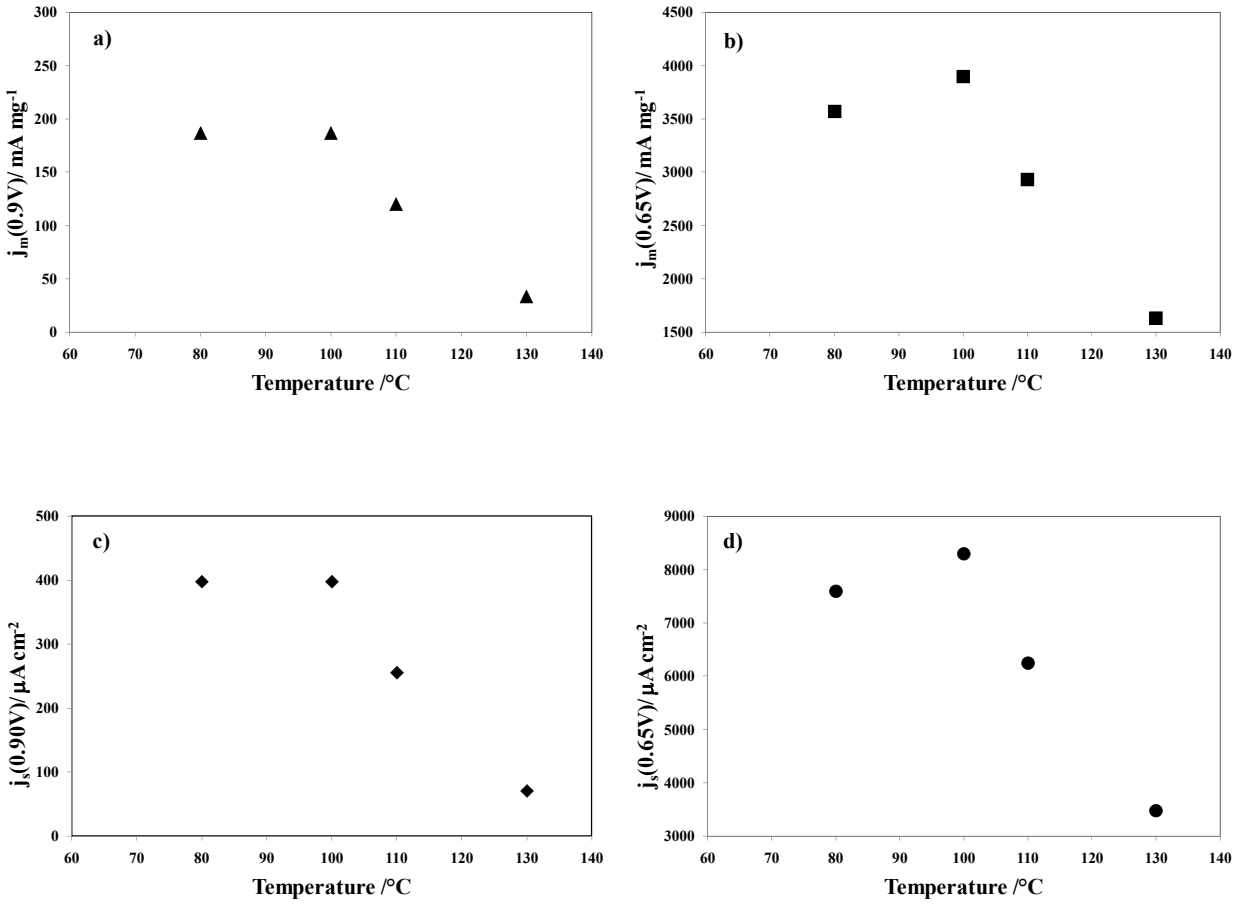
a)
$j_m$(0.9V)/ mA mg$^{-1}$
Temperature /°C
b)
$j_m$(0.65V)/mA mg$^{-1}$
Temperature /°C
c)
$j_s$(0.90V)/ µA cm$^{-2}$
Temperature /°C
d)
$j_s$(0.65V)/µA cm$^{-2}$
Temperature /°C

Figure 6a-d

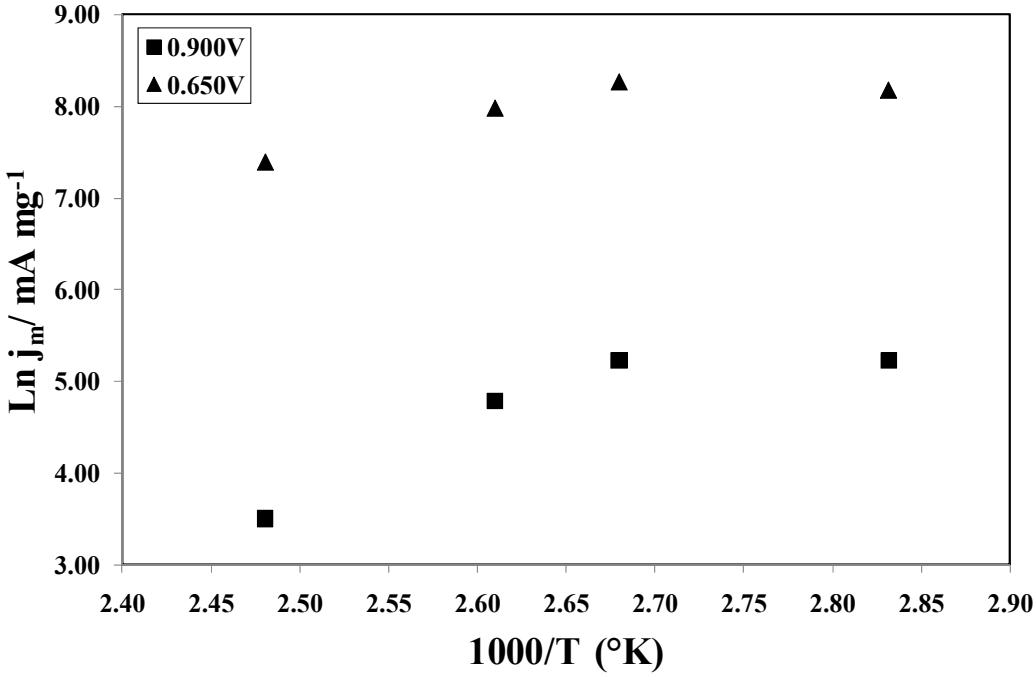
9.00
8.00
7.00
6.00
5.00
4.00
3.00
Ln $j_m$/ mA $mg^{-1}$
0.900V
0.650V
2.40
2.45
2.50
2.55
2.60
2.65
2.70
2.75
2.80
2.85
2.90
1000/T (°K)

Figure 7